Global vector-field reconstruction by using a multivariate polynomial L_2 approximation on nets

G. Gouesbet and C. Letellier

*Laboratoire d'Energétique des Systèmes et Procédés, Institut National des Sciences Appliquées de Rouen, Coria,
Boîte Postale 08 76131, Mont-Saint-Aignan Cedex, France*

A multivariate polynomial L_2 approximation on nets is designed for global vector-field reconstructions of time continuous dynamical systems. The technique is tested by investigating standard forms of the Rössler band, the Lorenz mask, and a chaotic attractor produced by a simple model of thermal lens oscillations.

I. INTRODUCTION

Global vector-field reconstruction is a topic of growing interest in the field of nonlinear dynamics with pioneering papers by Packard et al. [1], Crutchfield and McNamara [2], and Farmer and Sidorowich [3]. For time continuous dynamical systems, which are considered in this paper, a basic problem is, given a scalar time series for an observable, to provide a set of ordinary differential equations (ODE's) equivalent to the original underlying system. It is worthwhile to point out that such a problem may be at first sight a somewhat weird one because, when the aim is achieved, we own one ODE for the observable supplemented with ODE's for dynamical variables on which no observation has been made. The possibility of such a somewhat intriguing achievement results from mathematical works by Whitney [4,5], Mañé [6], and Takens [7,8]. For instance, let us consider a strange attractor of typical fractal dimension D embedded in a minimal phase space of dimension n_0 (then $D \leq n_0$). Takens's theorem states that the attractor may be generically reconstructed in a phase space of dimension $n \geq n_T$ in which $n_T = 2D + 1$ (ideally, D would refer to the Hausdorff dimension of the set). Here, the word generically means that using $n \geq n_T$ is in principle always sufficient to reconstruct the attractor. This theorem is routinely used for numerical evaluations of invariants, relying for instance on the so-called time-delay method, by studying reconstructed attractors diffeomorphically related to the original attractor. Of course, reconstruction phase spaces of dimension $n < n_T$ may also work. In particular, global vector-field reconstructions discussed in this paper use a minimal phase space of dimension n_0. Beside providing algorithms to construct phenomenological models from numerical scalar time series, global vector-field reconstructions provide many opportunities previously discussed ([9–13]), one of them being the forecasting of the observable. More generally, many comments and discussions available from Refs. [9–13] are not repeated in this paper in which attention is focused on new results.

One possibility for global vector-field reconstructions is to use a time-delay technique associated with a singular value decomposition (SVD) to choose the appropriate dependent variables appearing in the dynamical equations. This method leads to the research of approximate functions to model eigenfunctions generated by the SVD [14,15]. A typical claim is that SVD has the advantage of providing an efficient filter for the noise which is always present in experimental data. Following Palus and Dvorák [16], however, this claim must seemingly be softened. In Ref. [16] it is in particular demonstrated that the detected noise level and even its occurrence in a singular spectrum depend on the time delay used in the time-delay embedding rather than on the actual amount of noise in the data. The authors conclude that using SVD as a noise rejection technique by rejecting noisy components of the embedding in the basis of singular vectors is dubious and that, seemingly, SVD can reduce dynamical information rather than noise.

More generally, global vector-field reconstructions are feasible by using any kinds of embedding techniques, such as those discussed by Mindlin et al. [17]. Beside time-delay embedding previously discussed in connection with SVD, integral filters and differential embeddings may be used. A good review of these different methods is given by Casdagli et al. [18]. In a more recent paper, Gibson et al. clarify the mathematical relationships between them [19].

In our previous contributions to the topic of global vector-field reconstructions [9–13] we have used differential embeddings by using the scalar observable and successive derivatives. The reconstructed system of ODE's then takes a simple form that we call the standard system (or canonical system following Mindlin et al. terminology) exhibiting a single unknown function F called the standard (or canonical) function. By using the available scalar time series of the observable, we are then left with the problem of evaluating the standard function F within the framework of the theory of approximation of functions [20].

To solve this problem, we must start by choosing a model for the function F, then involved parameters must be evaluated for instance by using L_2 approximations, i.e., least-squares methods. We previously retained rational functions (ratios of multivariate polynomials) to model the standard function F, and successfully reconstructed ODE's generating Rössler and Lorenz chaotic attractors, with variable x taken as the observable. Rational functions present the advantage of allowing one to

model standard functions with poles, which is indeed found to be the case for the Rössler and Lorenz standard systems when x is the observable. However, the existence of such poles in the model leads to two difficulties. The first one is that, when integrating the standard ODE's, trajectories must cross singular sets that, although of Lebesgue measure 0, lead to numerical instabilities requiring special procedures (see Refs. [9,10,12] for details). Second, these singular sets have been found to produce a lack of robustness with respect to the presence of noise (unpublished). Furthermore, no general theorem of convergence is known for rational functions.

Therefore, new advances have required the implementation of a more robust method to approximate the standard function F. This paper is devoted to such a method, namely, the use of multivariate polynomial L_2 approximations on nets. For polynomial approximations, we own a convergence theorem, the so-called Weierstrass theorem [20]. The method is more robust than using rational functions due to the absence of poles, and it will be shown that polynomial approximations without any pole may correctly model exact standard functions with poles. Simple dynamics like periodic ones may be investigated by our method. However, this paper will only study chaotic dynamics providing more acid test cases. The nets on which polynomials are built are then chaotic nets generated by the attractor natural measure. Polynomials are not a priori chosen as Legendre polynomials in the work by Cremers and Hübler [21], but are specific to the attractor under study and actually provide a signature of it. Also, unknown parameters are not determined from a χ^2 optimization as in Refs. [2,15], or [22], but may be evaluated sequentially.

Although this paper only discusses differential embeddings, let us note that the presented approximation technique may also be used for other kinds of embeddings; for instance, to model eigenfunctions generated by SVD. It is also suggested here that global vector-field reconstructions might benefit from coupling different kinds of embeddings. For instance, after noise reduction by using a time-delay method with SVD, a clean scalar time series could be generated and used to construct differential embeddings. The case of noisy signals is however not considered in this paper.

The material is organized as follows. Section II recalls the basic ingredients of our method of global vector-field reconstructions by using standard functions and introduces the test cases to be investigated. Section III solves a mathematical exercise required for further use, while Sec. IV develops the formulation of our multivariate polynomial approximation technique. Test-case results are presented in Sec. V. Section VI is a conclusion.

II. STANDARD SYSTEMS AND TEST CASES

A. Standard systems, standard functions, and associated transformations

Let us consider a time continuous dynamical system defined by a set of ODE's,

$$\frac{d\mathbf{x}}{dt} \equiv \dot{\mathbf{x}} = f(\mathbf{x};\mu) , \tag{1}$$

in which $\mathbf{x}(t) \in \mathbb{R}^n$ is a vector valued function depending on a parameter t called the time, and f, the so-called vector field, is an n-component smooth function generating a flow ϕ_t (see Ref. [23]). $\mu \in \mathbb{R}^p$ is the parameter vector with p components, assumed to be constant in this paper. The system (1) is called the original system (OS). Without any loss of generality, we shall take $n = 3$ in this paper. The OS may therefore be written as

$$\dot{x}_1 = f_1(x_1, x_2, x_3) ,$$
$$\dot{x}_2 = f_2(x_1, x_2, x_3) , \tag{2}$$
$$\dot{x}_3 = f_3(x_1, x_2, x_3) .$$

It is then assumed that the observer numerically (or experimentally) recorded a scalar time signal. By convention, the observable is taken to be x_1, leading to a sampled scalar time series $\{x_1^i\}_{i=1}^{N_q}$, in which the integer i denotes discrete times.

The aim is thereafter to reconstruct a vector-field equivalent (in some sense) to the OS under the form of a standard system (SS) made of the observable and of its derivatives according to

$$\dot{y}_1 = \dot{x}_1 = y_2, \quad \dot{y}_2 = y_3, \quad \dot{y}_3 = F(x_1, y_2, y_3) , \tag{3}$$

in which the SS phase space is spanned by standard coordinates (y_1, y_2, y_3) with $y_1 \equiv x_1$. When only the time series $\{x_1^i\}_{i=1}^{N_q}$ is known, the knowledge of the number of equations (and derivatives) to be introduced in the SS must be independently obtained as discussed in Refs. [9–12]. In Ref. [13] it has also been stated that Refs. [9–12] heuristically commented on the existence of SS's but that a complete study of this problem was postponed to future work. Actually, this problem might be much simpler than we thought as explained below. Let us consider the attractor A_{OS} of the OS defined by $x_1(t), x_2(t), x_3(t)$ and introduce the direct standard transformation (DST) expressing the standard coordinates $\{y_i\}$ versus the original coordinates x_i. We have

$$y_1 = x_1, \quad y_2 = f_1(x_1, x_2, x_3), \quad y_3 = \sum_{j=1}^{3} \frac{\partial f_1}{\partial x_j} f_j . \tag{4}$$

Therefore, the DST is a well defined transformation without any singularity since the original vector field (f_1, f_2, f_3) is smooth. Hence A_{OS} is mapped by the DST to the attractor A_{SS} of the SS. The existence of A_{SS} implies that there must exist one standard function $F(y_i)$, at least an approximate one. When the OS is known, algebraic manipulations in principle allow one to find the standard function $F(y_i)$ more specifically called here the standard exact function (SEF). The SS in which F is the SEF is called the standard exact system (SES). Examples in Refs. [9–13] and in this paper show that in practice the SEF may be difficult or even impossible to derive, or may contain singularities. The existence of the A_{SS} implies that these singularities must likely be pseudosingularities, as discussed in Refs. [9–13]. Obviously, the method will fail if variables are not coupled, as discussed

in Ref. [11]. In such a case, measurements on one variable cannot provide information on hidden variables. In the present work, however, coupling is assumed to exist (in a nonlinear way). A general rigorous mathematical framework associated with these statements remains to be derived.

The nature of the equivalence between the original and the reconstructed attractors has been clarified in terms of (i) a diffeomorphic equivalence and (ii) a topological equivalence by using knot theory and templates. The details will appear elsewhere.

We also introduce the inverse standard transformation (IST) expressing the original coordinates versus the standard coordinates which may also be derived when the OS is known. By manipulating the examples later discussed in this section, the reader will remark that in practice the IST may also be very difficult or even impossible to derive, or may contain (pseudo) singularities. Actually, a bit of algebra shows that deriving the IST is a prerequisite to finding the SEF. Therefore, difficulties associated with the IST are conveyed to the SEF.

Such difficulties associated with the IST and the SEF should not prevent A_{SS} to exist as previously mentioned, due to the properties of the DST. Therefore, instead of looking for the SEF, we may look for an accurate enough approximation F^* to F. In particular, when the OS is unknown, the SEF cannot be found and global vector-field reconstruction with differential embeddings are obtained if accurate enough F^*'s are built. The procedure is as follows.

Simultaneously to the sampled scalar time series $\{x_1^i\}_{i=1}^{N_q}$, vectorial time series $\{y_1^i = x_1^i, y_2^i = \dot{x}_1^i, y_3^i = \ddot{x}_1^i, \dot{y}_3^i = \dddot{x}_1^i\}_{i=1}^{N_q}$ may be obtained by using an accurate enough finite-difference scheme. In practice we used a centered second order scheme as discussed in our previous works. Let us, however, note the possibility of using discrete linear filters based on discrete Legendre polynomials, generalizing finite differencing [19]. The set $\{y_1^i, y_2^i, y_3^i\}_{i=1}^{N_q}$ is called a net, and N_q is therefore the net size. With each point of the net is associated a value $\{\dot{y}_3^i\}$. The last equation in (3) shows that we are then left with a fitting problem to evaluate an approximation F^* to F. Once this problem is solved, we own a standard reconstructed function F^* (SRF) that, when incorporated in the SS, provides a standard reconstructed system (SRS). In the limit of a perfect reconstruction, the attractors generated by the SES and by the SRS must be identical. The aim of this paper is to implement a new technique to build SRF's (Secs. III and IV) and to test it on test cases which are now presented.

B. Rössler system

For the Rössler system, there are three original coordinates (x, y, z). Each of these coordinates may be taken as the observable, and therefore three different cases can be investigated.

1. Observable x

The OS reads

$$\dot{x} = -y - z, \quad \dot{y} = x + ay, \quad \dot{z} = b + z(x - c) , \qquad (5)$$

with a control parameter vector $a, b, c = 0.398, 2, 4$ for which the asymptotic motion settles down to a strange chaotic attractor [24]; i.e., original coordinates are $x_1, x_2, x_3 = x, y, z$ with x being the observable.

The standard system reads

$$\dot{x} = Y, \quad \dot{Y} = Z, \quad \dot{Z} = F(x, Y, Z) , \qquad (6)$$

in which standard coordinates y_1, y_2, y_3 are x, Y, Z.

The DST reads

$$x = x, \quad Y = -y - z, \quad Z = -b - x - ay + z(c - x) . \qquad (7)$$

The IST is found to be

$$x = x ,$$

$$y = -\frac{Y(c - x) + Z + b + x}{a + c - x} , \qquad (8)$$

$$z = \frac{Z + b + x - aY}{a + c - x} ,$$

while the SEF reads

$$\dot{Z} = ab - cx + x^2 - axY + xZ + (ac - 1)Y$$

$$+ (a - c)Z - \frac{Y(x + b - aY + Z)}{a + c - x} . \qquad (9)$$

This is a case in which the IST and the SEF exhibit a set of (pseudo) singularities $x_c = (a + c)$ of Lebesgue measure 0. The status of this set and numerical consequences when integrating the SES are discussed in Refs. [9,10]. Successful reconstructions are obtained by using a model of rational functions for the SRF [9,10,13]. The mathematical structure of such a model, however, fits perfectly the SEF which is indeed a rational function.

2. Observable y

Using a cyclic permutation over coordinates (x, y, z), original coordinates are now taken to be (y, z, x) and standard coordinates are (y, Z, X) with a standard function $\dot{X} = F(y, Z, X)$. The DST then reads

$$y = y, \quad Z = x + ay, \quad X = ax + (a^2 - 1)y - z . \qquad (10)$$

The IST is

$$y = y, \quad z = aZ - X - y, \quad x = Z - ay , \qquad (11)$$

and the SEF reads

$$\dot{X} = -b + (a - c)X - cy + (ac - 1)Z - ay^2$$

$$- aZ^2 - aXy + XZ + (a^2 + 1)yZ . \qquad (12)$$

This is a very simple case where no singularity appears in the IST nor in the SEF. A rational function model as in our previous works would be quite suited for this case where the SEF exhibits a polynomial structure. It will also provide a nice checking of the polynomial model to be discussed later and of associated computer programs.

3. Observable z

Pursuing with the cyclic permutation, original coordinates are now (z, x, y) and standard coordinates are (z, X, Y) with standard function $\dot{Y} = F(z, X, Y)$. The DST reads

$z = z$,

$$X = b + z(x - c) ,$$ (13)

$$Y = -bc + bx + c^2 z - 2cxz - yz - z^2 + x^2 z .$$

The IST is found to be

$$z = z, \quad x = c + \frac{X - b}{z}, \quad y = -z - \frac{Y}{z} + \frac{X(X - b)}{z^2} ,$$ (14)

and the standard function reads

$$\dot{Y} = b - (X + c)z - X + aY + az^2 + \frac{1}{z}$$

$$\times [(ab + 3Y)X - bY - aX^2] + \frac{2X^2}{z^2}(b - X) .$$ (15)

This is again a rational function case that could be readily investigated by methods discussed in [9–13]. Let us note the appearance of a set of singularities for $z = 0$.

C. Lorenz system

Again, three cases may be considered.

1. Observable x

The OS reads

$$\dot{x} = \sigma(y - x), \quad \dot{y} = Rx - y - xz, \quad \dot{z} = -bz + xy ,$$ (16)

with a control parameter vector $(R, \sigma, b) = (28, 10, \frac{8}{3})$ for which the asymptotic motion settles down to a strange chaotic attractor [24,25]. Standard coordinates are taken to be (x, Y, Z). The DST reads

$$x = x, \quad Y = \sigma(y - x), \quad Z = \sigma[(R + \sigma)x - (\sigma + 1)y - xz] .$$ (17)

The IST is found to be

$$x = x, \quad y = x + \frac{Y}{\sigma}, \quad z = (R - 1) - \frac{1}{\sigma x}[(\sigma + 1)Y + Z] ,$$ (18)

while the SEF reads

$$\dot{Z} = b\sigma(R - 1)x - b(\sigma + 1)Y - (b + \sigma + 1)Z$$

$$- x^2 Y - \sigma x^3 + \frac{Y[(\sigma + 1)Y + Z]}{x} .$$ (19)

This is again a rational function case in which the IST and the SEF exhibit singularities for $x = 0$. The use of a rational function model is discussed in Refs. [11–13].

2. Observable y

Using again cyclic permutations, original coordinates are y, z, x and standard coordinates are denoted by (y, Z, X). The DST reads

$y = y$,

$$Z = Rx - y - xz ,$$ (20)

$$X = -R(\sigma + 1)x + (R\sigma + 1)y$$

$$+ (\sigma + b + 1)xz - \sigma yz - x^2 y .$$

The research of the IST and of the SEF is however rather difficult for this case, requiring in particular one to solve an algebraic third-order equation in x^3 to express $x(y, Z, X)$. Although readily obtained by using symbolic computation software, the results are too involved to be given here. The SEF does not take the form of rational functions and exhibits singularities for $x = 0$ and $y = 0$.

3. Observable z

Original coordinates are now (z, x, y) and standard coordinates are (z, X, Y). The DST reads

$z = z$,

$$X = -bz + xy ,$$ (21)

$$Y = b^2 z + Rx^2 + \sigma y^2 - (b + \sigma + 1)xy - x^2 z .$$

The research of the IST and of the SEF is also rather complicated for this case, requiring in particular one to solve an algebraic fourth-order equation in x^4 to express $x(z, X, Y)$. This equation is however bisquared. Again, results are too involved to be presented here. The SEF does not take the form of rational functions and exhibits singularities at least for $z = R$.

D. Thermal lens oscillations

In trying to understand thermal lens oscillations (TLO's) and associated hot-wire experiments ([26,27] and references therein), a so-called simple model leading to a three-dimensional (3D) dynamical system has been developed [28]. Strange chaotic attractors are produced by this TLO model. For instance, let us consider the following dynamical system leading to the chaotic attractor in Fig. 9, Ref. [28]:

$$\dot{x} = y ,$$

$$\dot{y} = [R(1 + x)(1 + z) - 1]y$$

$$- [R(1 + x)(1 + z)]^{1.40}(\sinh y - y)$$

$$- \left| \frac{2\pi R(1 + x)(1 + z)}{R(1 + x)(1 + z) + 1} \right|^2 \sinh x ,$$ (22)

$$\dot{z} = S \left[1 - \frac{1 + z}{(1 + x)^2} \right] - (R - 1)^{1/2}|y|^{1/2}(1 + z^{5001}) ,$$

in which

$$R = 10.1696, \quad S = 2^{0.70} .$$ (23)

The exponent (5001) in Eqs. (22) provides a sharp cutoff corresponding in the physical model to a transition between convective and diffusive heat transfer. The precise value of this exponent is not essential, but it must be great and odd. Due to the sharp cutoff and to the com-

plicated structure of the vector field, this model is expect-
ed to provide a very acid test for global vector-field
reconstruction techniques.

With standard coordinates (x, Y, Z), the DST is readily
found to be

$$x = x, \quad Y = y, \quad Z = \sum_{j=1}^{3} \frac{\partial f_1}{\partial x_j} f_j = \ddot{y} \ . \tag{24}$$

However, the research of the IST and of the SEF leads to
tremendous technical difficulties that we were not able to
solve with a reasonable effort.

III. MATHEMATICAL PRELIMINARIES

The polynomial approximation method in this paper
will use polynomials denoted ϕ^p, $p \in \{1, 2, \ldots\}$, depend-
ing on three standard coordinates y_1, y_2, y_3, therefore in-
volving terms reading y_1^j, y_2^u, y_3^v, $j, u, v \in 0, 1, 2, \ldots$.
Hence an explicit biunivocal correspondence (BC) be-
tween integers p and triplets (j, u, v) denoted $p \leftrightarrow (j, u, v)$
will be useful. Establishing such a BC is conveniently car-
ried out in two steps.

A. First step

We start by establishing a BC $p \leftrightarrow (u, v)$ between in-
tegers $p \in 1, 2, \ldots$ and doublets (u, v), $u, v \in 0, 1, 2, \ldots$.
There are infinitely many such BC's because N is equipo-
tent to N^2 (and more generally to N^n). However, to serve
our later purpose, we choose a BC obtained by arranging
doublets (u, v) in lines according to

$$(0,0) \quad \text{line 1} \ ,$$
$$(1,0), (0,1) \quad \text{line 2} \ , \tag{25}$$
$$(2,0), (1,1), (0,2) \quad \text{line 3} \ ,$$

and numbering them sequentially according to the
scheme

$$1 \quad \text{line 1} \ ,$$
$$2, 3 \quad \text{line 2} \ , \tag{26}$$
$$4, 5, 6 \quad \text{line 3} \ .$$

Let us consider one integer p in (26) and ask which is
the corresponding doublet (u, v). It is an exercise to show
that the question may be answered by applying the fol-
lowing algorithm.

(i) Evaluate n complying with

$$\frac{n(n+1)}{2} < p < \frac{(n+1)(n+2)}{2} + 1 \ . \tag{27}$$

(ii) Let us set

$$k = p - \frac{n(n+1)}{2} \ . \tag{28}$$

(iii) Then

$$(u, v) = (n - k + 1, k - 1) \ . \tag{29}$$

Conversely, let (u, v) be given. It is again an exercise to
establish that

$$p = \frac{(u+v)(u+v+1)}{2} + (v+1) \ . \tag{30}$$

Equation (30) is very convenient for numerical evalua-
tion but (27) involving inequalities is not. The reader
may however establish that the algorithm (27)–(29) may
be replaced by a fully explicit one, evaluating n according
to

$$x = \frac{-1 + (8p - 3)^{1/2}}{2} \ , \tag{31}$$

$$n = \text{int}(x) \ . \tag{32}$$

B. Second step

Doublets (u, v) with $p \leftrightarrow (u, v)$ having been defined in
Sec. III A, let us now construct triplets (j, u, v). Let us as-
sume that we have constructed all triplets (j, u, v) such
that $(j + u + v) \leq (N - 1)$ and that we are going to con-
struct all the triplets such that $(j + u + v) = N$.

The number of triplets with $(j + u + v) \leq (N - 1)$ is
found to be

$$n_{N-1} = \begin{bmatrix} N+2 \\ 3 \end{bmatrix} \ . \tag{33}$$

The number of triplets with $(j + u + v) \leq N$ is similarly

$$n_N = \begin{bmatrix} N+3 \\ 3 \end{bmatrix} \ . \tag{34}$$

Therefore the number of triplets with $(j + u + v) = N$ we
have to construct is

$$n_c = \begin{bmatrix} N+3 \\ 3 \end{bmatrix} - \begin{bmatrix} N+2 \\ 3 \end{bmatrix} = \frac{(N+1)(N+2)}{2}$$

$$= \begin{bmatrix} N+2 \\ 2 \end{bmatrix} \ , \tag{35}$$

which is equal to the number of doublets (u, v) with
$(u + v) \leq N$. Therefore, all triplets with $(j + u + v) = N$
may be obtained from doublets (u, v) with $(u + v) \leq N$ by
adding a first integer j according to the following scheme.

(i) Add integer N to all doublets (u, v) with $(u + v) = 0$,
to produce triplets (N, u, v) with $(j + u + v) = N$.

(ii) Add integer $(N - 1)$ to all doublets (u, v) with
$(u + v) = 1$ to produce triplets $(N - 1, u, v)$ with
$(j + u + v) = N$, etc., ending with the following.

(iii) Add integer 0 to all doublets (u, v) with
$(u + v) = N$ to produce triplets $(0, u, v)$ with $(j + u$
$+ v) = N$.

Therefore, in any case, we have $(j + u + v) = N$ as re-
quired. Each constructed triplet is different from all oth-
ers and the construction ensures that the number of trip-
lets with $(j + u + v) = N$ is equal to the number of dou-
blets with $(u + v) \leq N$, i.e., equal to $\binom{N+2}{2}$ as required by
Eq. (35). Hence, our construction is perfect.

To gain a better insight into this construction method,
let us examine how it works for the first values of N, con-
sidering doublets given in Eq. (25). Triplets (j, u, v) with
$(j + u + v) = 0$ have only one parent $(0,0)$ to which we add
a first integer $N = 0$ to generate $(0,0,0)$. Triplets (j, u, v)

with $j+u+v)=1$ have three parents, the doublet $(0,0)$ with $(u+v)=0$ to which we add $N=1$ to obtain $(1,0,0)$ and doublets $(1,0)(0,1)$ with $(u+v)=1$ to which we add $(N-1)=0$ to obtain $(0,1,0)$ and $(0,0,1)$. Similarly, triplets (j,u,v) with $(j+u+v)=2$ have six parents, one $(0,0)$ with $(u+v)=0$ in line 1 of (25), two with $(u+v)=1$ in line 2, and three with $(u+v)=2$ in line 3.

The resulting triplets may be arranged in lines with $(j+u+v)=cst$ in a line, and each line may be subdivided into sublines such as $(u+v)=cst$ in a subline leading to the following pattern:

$$
\begin{array}{lll}
(0,0,0) & & \text{line 1} \\
\\
(1,0,0) & & \\
(0,1,0),\ (0,0,1) & & \text{line 2} \\
\\
(2,0,0) & & \\
(1,1,0),\ (1,0,1) & & \text{line 3} \\
(0,2,0),\ (0,1,1),\ (0,0,2) & & \\
\vdots & &
\end{array}
\tag{36}
$$

clearly illustrating the construction method. The BC: $p\leftrightarrow(j,u,v)$ is then defined by sequentially numbering the triplets in (36) according to

$$
\begin{array}{ll}
1 & \text{line 1} \\
\\
2 & \\
 & \text{line 2} \\
3\ 4 & \\
\\
5 & \\
6\ 7 & \text{line 3} \\
8\ 9\ 10 & \\
\vdots &
\end{array}
\tag{37}
$$

From (36) and (37), the BC, $p\leftrightarrow(j,u,v)$, may be explicitly written down. This is a rather tedious exercise which is left to the reader. Results are however given below.

Let p be given. Then the triplet (j,u,v) is found by applying the following algorithm.

(i) Evaluate N satisfying

$$
\begin{bmatrix} N+2 \\ 3 \end{bmatrix} < p < \begin{bmatrix} N+3 \\ 3 \end{bmatrix} + 1 \ .
\tag{38}
$$

(ii) Evaluate j satisfying

$$
\begin{bmatrix} N+2 \\ 3 \end{bmatrix} + \begin{bmatrix} N-j+1 \\ 2 \end{bmatrix} < p
$$
$$
< \begin{bmatrix} N+3 \\ 3 \end{bmatrix} + \begin{bmatrix} N-j+2 \\ 2 \end{bmatrix} + 1 \ .
\tag{39}
$$

(iii) Then

$$
k = p - \begin{bmatrix} N+2 \\ 3 \end{bmatrix} - \begin{bmatrix} N-j+1 \\ 2 \end{bmatrix} \ .
\tag{40}
$$

(iv) And

$$
u = N - j - k + 1 \ ,
\tag{41}
$$

$$
v = k - 1 \ .
\tag{42}
$$

Equations (38) and (39), which evaluate N and j, are numerically inefficient because they involve inequalities. It is left to the reader to demonstrate that they may be replaced by the following set of formulas:

$$
a = 6(p - \epsilon_1) \ ,
\tag{43}
$$

$$
x = \left[\frac{a}{2} + \frac{(27a^2-4)^{1/2}}{6\sqrt{3}} \right]^{1/3}
$$
$$
+ \left[\frac{a}{2} - \frac{(27a^2-4)^{1/2}}{6\sqrt{3}} \right]^{1/3} - 1 \ ,
\tag{44}
$$

$$
N = \text{int}(x) \ ,
\tag{45}
$$

$$
\Delta = (2N+1)^2 - 4\left[\frac{N(N+1)(N+5)}{3} - 2(p - \epsilon_2) \right] \ ,
\tag{46}
$$

$$
y = \frac{2N+1-\Delta^{1/2}}{2} \ ,
\tag{47}
$$

$$
j = \text{int}(y+1) \ .
\tag{48}
$$

Conversely, let (j,u,v) be given. Then we have

$$
p = \begin{bmatrix} j+u+v+2 \\ 3 \end{bmatrix} + \begin{bmatrix} u+v+1 \\ 2 \end{bmatrix} + \begin{bmatrix} v+1 \\ 1 \end{bmatrix} \ .
\tag{49}
$$

In Eqs. (43) and (46), ϵ_1 and ϵ_2 must comply with

$$
0 < \epsilon_1, \epsilon_2 < 1 \ .
\tag{50}
$$

Numerical checking of the algorithm leads us to recommend $\epsilon_1 = \epsilon_2 = 0.3$. On a Stardent 3000 computer, the algorithm then works perfectly well up to $p \approx 10^6$.

IV. POLYNOMIAL APPROXIMATION TECHNIQUE

A. Complete multivariate basis of polynomials

We introduce the notation

$$
y_1^j y_2^u y_3^v = (y_1 y_2 y_3)^p \ ,
\tag{51}
$$

in which $p\leftrightarrow(j,u,v)$ according to the BC introduced in Sec. III. Then, we introduce a multivariate family of polynomials ϕ^k, $k \in 1,2,\ldots$:

$$
\phi^k = \sum_{n=1}^{k} A_n^k (y_1 y_2 y_3)^n \ .
\tag{52}
$$

The first members of the family read

$$
\phi^1 = A_1^1 \ ,
\tag{53}
$$

$$
\phi^2 = A_1^2 + A_2^2 y_1 \ ,
\tag{54}
$$

$$
\phi^3 = A_1^3 + A_2^3 y_1 + A_3^3 y_2 \ ,
\tag{55}
$$

$$
\phi^4 = A_1^4 + A_2^4 y_1 + A_3^4 y_2 + A_4^4 y_3 \ ,
\tag{56}
$$

$$
\phi^5 = A_1^5 + A_2^5 y_1 + A_3^5 y_2 + A_4^5 y_3 + A_4^5 y_1^2 \ ,
\tag{57}
$$

$$
\vdots
$$

showing that the BC, $p \leftrightarrow (j,u,v)$, generates a multivariate triangle family of polynomials generalizing the monovariable case discussed in Ref. [29]. Coefficients A_n^n on the upper border of the triangle are called leading coefficients (LC's). Monomials $(y_1 y_2 y_3)^n$ may then be determined uniquely and recursively from linear combinations of ϕ^k's. For instance,

$$(y_1 y_2 y_3)^1 = y_1^0 y_2^0 y_3^0 = \frac{\phi^1}{A_1^1} = B_1^1 \phi^1 , \tag{58}$$

$$(y_1 y_2 y_3)^2 = y_1^1 y_2^0 y_3^0 = \frac{1}{A_2^2} \left[\phi^2 - \frac{A_1^2}{A_1^1} \phi^1 \right]$$

$$= B_1^2 \phi^1 + B_2^2 \phi^2 . \tag{59}$$

More generally, we have

$$(y_1 y_2 y_3)^k = \sum_{n=1}^{k} B_n^k \phi^n . \tag{60}$$

Clearly, the family ϕ^k is only usable if we demand $A_n^n \neq 0$ for all n. Let us now consider a multivariate polynomial $P(y_1, y_2, y_3)$:

$$P(y_1, y_2, y_3) = \sum_{k=1}^{N} c_k (y_1 y_2 y_3)^k . \tag{61}$$

With $N \leftrightarrow (N_1, N_2, N_3)$, partial degrees with respect to y_1, y_2, y_3 are N_1, N_2, N_3, respectively. By using (60), Eq. (61) may be rewritten as

$$P(y_1, y_2, y_3) = \sum_{i=1}^{N} d_i \phi^i . \tag{62}$$

Therefore the family $\phi^1, \ldots, \phi^N$ forms a complete basis for all polynomials up to degrees N_1, N_2, N_3 with respect to y_1, y_2, y_3. In the limit $N \rightarrow \infty$, we obtain a complete basis for all 3D polynomials.

B. Orthogonalization

We now design an orthogonal triangle family of polynomials. It will be found that the construction of the family is unique except for the values of the LC's. However, contrasting with 1D case [29], it is not possible to express ϕ^j from ϕ^k's, $k < j$, by using a recurrence relation.

It is assumed that the family has been built up to n, i.e., we own $\phi^1, \ldots, \phi^n$ with ϕ^i orthogonal to ϕ^j, for all i and for all $j \neq i$. Therefore, coefficients $A_1^1, A_1^2, A_2^2, \ldots,$ $A_1^n, \ldots, A_n^n$ and $B_1^1, B_1^2, B_2^2, \ldots, B_1^n, \ldots, B_n^n$ are known. We now build ϕ^{n+1} given by

$$\phi^{n+1} = \sum_{i=1}^{n+1} A_i^{n+1} (y_1 y_2 y_3)^i . \tag{63}$$

Setting

$$A_{n+1}^{n+1} = \alpha_n A_n^n \tag{64}$$

with arbitrary values of $\alpha_n \neq 0$, we have

$$\phi^{n+1} = \sum_{i=1}^{n} A_i^{n+1} (y_1 y_2 y_3)^i + \alpha_n A_n^n (y_1 y_2 y_3)^{n+1} , \tag{65}$$

i.e., we must evaluate n coefficients A_i^{n+1} knowing n

orthogonality relations. Using Eq. (60), Eq. (65) may be rewritten as

$$\phi^{n+1} = \sum_{i=1}^{n} \sum_{j=1}^{i} A_i^{n+1} B_j^i \phi^j + \alpha_n A_n^n (y_1 y_2 y_3)^{n+1} . \tag{66}$$

Let us introduce an inner product $(\ , \ )$ to be defined later and write the orthogonality condition

$$(\phi^{n+1}, \phi^n) = 0 . \tag{67}$$

Equation (66) then readily leads to

$$A_n^{n+1} = \frac{-\alpha_n A_n^n ((y_1 y_2 y_3)^{n+1}, \phi^n)}{B_n^n (\phi^n, \phi^n)} . \tag{68}$$

Similarly, writing successively the orthogonality conditions

$$(\phi^{n+1}, \phi^{n-k}) = 0, \quad k = 1, 2, \ldots, n-1 \tag{69}$$

we recursively obtain

$$A_{n-k}^{n+1} = \frac{1}{B_{n-k}^{n-k}} \left[\frac{-\alpha_n A_n^n ((y_1 y_2 y_3)^{n+1}, \phi^{n-k})}{(\phi^{n-k}, \phi^{n-k})} - \sum_{i=n-k+1}^{n} A_i^{n+1} B_{n-k}^i \right]$$

$$k = 1, 2, \ldots, n-1 . \tag{70}$$

The orthogonalization scheme must be completed by providing companion relations to evaluate the coefficients B_j^i appearing in Eqs. (68) and (70). Equation (52) may be rewritten as

$$\phi^k = \sum_{i=1}^{k-1} A_i^k (y_1 y_2 y_3)^i + A_k^k (y_1 y_2 y_3)^k , \tag{71}$$

which, together with Eq. (60), implies

$$B_k^k \phi^k + \sum_{\alpha=1}^{k-1} B_\alpha^k \phi^\alpha = \frac{1}{A_k^k} \left[\phi^k - \sum_{i=1}^{k-1} \sum_{\alpha=1}^{i} A_i^k B_\alpha^i \phi^\alpha \right] , \tag{72}$$

leading immediately to

$$B_k^k = \frac{1}{A_k^k} , \tag{73}$$

$$\sum_{\alpha=1}^{k-1} B_\alpha^k \phi^\alpha = -B_k^k \sum_{i=1}^{k-1} \sum_{\alpha=1}^{i} A_i^k B_\alpha^i \phi^\alpha . \tag{74}$$

Taking the inner product of (74) with ϕ^r, and using orthogonality, then lead to

$$B_r^k = -B_k^k \sum_{i=r}^{k-1} A_i^k B_r^i, \quad r = 1, \ldots, k-1 , \tag{75}$$

completing the scheme. In practice, because LC's are left arbitrary, we have chosen

$$A_k^k = 1 , \tag{76}$$

i.e., we also have

$$\alpha_k = B_k^k = 1 , \tag{77}$$

leading to trivial but useful simplifications. A somewhat equivalent Gram-Schmidt procedure to produce an orthonormal basis will be discussed elsewhere.

C. Inner product

Let us consider the net $\{y_1^i, y_2^i, y_3^i\}_{i=1}^{N_q}$ generated by the standard coordinates as defined in Sec. II A and two functions $G(y_1, y_2, y_3)$, $H(y_1, y_2, y_3)$ defined on this net. We introduce

$$(G, H) = \sum_{i=1}^{N_q} G(y_1^i, y_2^i, y_3^i) H(y_1^i, y_2^i, y_3^i)$$

$$\equiv \sum_{net} GH . \tag{78}$$

It is then an exercise to check that (G, H) is indeed satisfying properties required for an inner product [29]. This is the definition to be used in this paper. Furthermore, we have

$$(G, G) = \|G\|^2 , \tag{79}$$

in which $\| \|$ is a seminorm [29].

D. Fourier coefficients

By using the inner product (78), Secs. IV A and IV B provide a formulation to build a complete orthogonal family of multivariate polynomials ϕ^k. These polynomials are not a priori defined but generated by the net, i.e., by the natural measure of the attractor. We are now looking for an approximation F^* of the standard function which is known at the net points:

$$\dot{y}_3^i = F(y_1^i, y_2^i, y_3^i), \quad i \in [1, \ldots, N_q] . \tag{80}$$

The approximation F^* is researched as an expansion over polynomials ϕ^k according to

$$F^* = \sum_{j=1}^{N_p} c_j^* \phi^j . \tag{81}$$

A best L_2 approximation (in the least-squares sense) is obtained when $(F^* - F)$ is orthogonal to all the ϕ^k's (see Ref. [29]). Therefore, the condition is

$$\left(\sum_{j=1}^{N_p} c_j^* \phi^j - F, \phi^k \right) = 0, \quad k = 1, 2, \ldots . \tag{82}$$

The orthogonality property of the polynomials ϕ^k then implies that the Fourier coefficients are given by

$$c_j^* = \frac{(F, \phi^j)}{(\phi^j, \phi^j)} = \frac{\sum_{i=1}^{N_q} \dot{y}_3^i \phi^j(y_1^i, y_2^i, y_3^i)}{(\phi^j, \phi^j)} . \tag{83}$$

A somewhat similar method for constructing basis polynomials is discussed by Giona, Lentini, and Cimagalli [30]. However, by not using BC's, the obtained formulation looks to be of great complexity, as stated by the authors. In particular, polynomials are denoted by using a number of subscripts equal to the number of variables making relationships fairly difficult to read. Further-

more, the obtained family of polynomials does not look like it forms a multivariate triangle family. Actually, however, the triangular character of the family does exist but is hidden by the notation. For instance, in Ref. [30], Eq. (16), the first members of a family in the 2D case would be formed by taking $\Pi^{00}, \Pi^{10}, \Pi^{11}, \Pi^{20}, \Pi^{21}, \Pi^{22}, \ldots$, in that order. Giona, Lentini, and Cimagalli [30] apply their method to the reconstruction of vectorial time series (not of scalar time series).

E. Number of allowed polynomials

With the definition (78) for the inner product, the number of allowed polynomials ϕ^k is not infinite but actually depends on the number of points in the net. Indeed, if we are allowed to build N_p polynomials, these polynomials must be linearly independent since they must be orthogonal. We recall that N_p polynomials ϕ^k are linearly independent if, by definition,

$$\sum_{j=1}^{N_p} c_j \phi^j = 0 \Longrightarrow c_j = 0 \quad \text{for all } j . \tag{84}$$

Equation (84) must hold for each point on the net and therefore represents N_q equations to be satisfied by N_p polynomials. Let us assume that we have built N_q polynomials according to our constructive algorithm. They are orthogonal and therefore linearly independent. Equation (84) generates N_q equations containing N_p polynomials at each net point. If we are trying to build a $(N_q + 1)$th polynomial, then Eq. (84) generates N_q equations containing $(N_q + 1)$ polynomials at each net point. Since there is now one more coefficient c_j than the number of equations, we deduce that the $(N_q + 1)$th polynomial is not linearly independent. Since it is not linearly independent but must be orthogonal, it must be zero. Then $(\phi^{N_q+1}, \phi^{N_q+1}) = 0$ and the algorithm of construction must stop due to the inner products appearing in the denominators. Therefore, for a net with N_q points, the construction must stop when $\phi^1, \phi^2, \ldots, \phi^{N_q}$ are built.

F. A set of spectra and interpretation

The presented formulation generates a set of spectra that is worthwhile discussing. The first spectrum is the spectrum of coefficients A_j^i defining the basis polynomials ϕ^k. It may be called the direct basis spectrum. It is an exercise, working by recurrence, to show that in the limit $N_q \to \infty$ the inner products (ϕ^n, ϕ^n) are proportional to N_q but that the direct basis spectrum and therefore the polynomials do not depend on N_q, only involving moments $\langle (y_1 y_2 y_3)^p \rangle$ in which the average $\langle \ \rangle$ is taken with respect to the natural measure of the attractor. For instance, it is readily shown that

$$A_1^2 = -\langle y_1 \rangle , \tag{85}$$

$$A_2^3 = \frac{\langle y_1 \rangle \langle y_2 \rangle - \langle y_1 y_2 \rangle}{\langle y_1^2 \rangle - \langle y_1 \rangle^2} . \tag{86}$$

In the 1D case, the matrices A_j^i and B_j^i may be comple-

mented by setting to zero the undefined elements, then leading to extended matrices $[A_j^i]$ and $[B_j^i]$ which are each other's inverse [29]. Therefore, the set of coefficients B_j^i forms a spectrum that may be called the inverse basis spectrum. Although the triangular matrices A_j^i and B_j^i are still companions essentially containing the same information and enjoying similar properties, the extended matrices $[A_j^i]$ and $[B_j^i]$ have not been found to be each other's inverse in the multivariate case [see Eqs. (73) and (75)].

From the basis spectra A_j^i and B_j^i, it is possible to define a compound basis spectrum C_j^i according to

$$
\begin{aligned}
C_j^i &= A_j^i, \quad i \geq j \\
C_j^i &= B_{N_q-j+1}^{N_q-i+1}, \quad i \leq j
\end{aligned}
\tag{87}
$$

with the remark that

$$
C_i^i = A_i^i = B_{N_q-i+1}^{N_q-i+1} = 1 .
\tag{88}
$$

From an aforementioned remark exemplified in Eqs. (85) and (86), it follows that all these basis spectra form signatures of the metric properties of the attractor with respect to the natural measure. However, because $y_2 = \dot{y}_1$ and $y_3 = \dot{y}_2$ for standard systems [Eq. (3)], they may also be expressed as describing the coupling between the original observable $x_1 = y_1$ and the phase velocity components $\dot{y}_1$ and $\dot{y}_2$.

The set $\{c_j^*\}$ of Fourier coefficients [Eq. (83)] forms the Fourier spectrum. Again, this spectrum does not depend on N_q in the limit $N_q \to \infty$. Equation (83) shows that it contains information on the coupling between the metric properties and the phase velocity component $\dot{y}_3$. For instance,

$$
c_1^* = \langle \dot{y}_3 \rangle ,
\tag{89}
$$

$$
c_2^* = \frac{\langle \dot{y}_3(y_1 - \langle y_1 \rangle) \rangle}{\langle (y_1 - \langle y_1 \rangle)^2 \rangle} .
\tag{90}
$$

Recalling again $y_2 = \dot{y}_1$ and $y_3 = \dot{y}_2$, it is seen that this spectrum describes the coupling between the original observable $x_1 = y_1$ and all phase velocity components $\dot{y}_1 \dot{y}_2 \dot{y}_3$. It therefore contains information on the coupling between $x_1 = y_1$ and $\dot{y}_1, \dot{y}_2$ present in the basis spectra, plus information on the coupling between $x_1 = y_1$ and $\dot{y}_3$, which is not present in the basis spectra. Also, because conversely $\dot{y}_3 = F(y_1, y_2, y_3)$, the Fourier spectrum may also be expressed only in terms of statistics with respect to moments taken from the natural measure. This discussion shows that all the previous spectra involve statistics that may be described either only in terms of moments $\langle (y_1 y_2 y_3)^p \rangle$ taken from the natural measure or in terms of coupling between the original observable and phase velocity components. The corresponding interplay between metric and dynamical properties in standard systems might be worth investigating later.

Finally, from Eqs. (81) and (52), it follows that the approximate standard function F^* may also be written as

$$
\begin{aligned}
F^* &= \sum_{i=1}^{N_p} \sum_{j=1}^{i} c_i^* A_j^i (y_1 y_2 y_3)^j \\
&= \sum_{j=1}^{N_p} \sum_{i=j}^{N_p} c_i^* A_j^i (y_1 y_2 y_3)^j ,
\end{aligned}
\tag{91}
$$

leading to

$$
F^* = \sum_{j=1}^{N_p} K_j (y_1 y_2 y_3)^j
\tag{92}
$$

with

$$
K_j = \sum_{i=j}^{N_p} c_i^* A_j^i .
\tag{93}
$$

The form (92) is the most efficient for integrating the standard reconstructed function F^*. It shows that all information required to know the standard reconstructed vector field is actually contained in a number of coefficients K_j equal to N_p, the number of polynomials. If N_p is small for a successful reconstruction, then the chaotic trajectory will be encoded in a small set of values. This set may be called the standard polynomial spectrum or, in short, the K spectrum. It provides the most concise signature of the attractor. Graphical displays of spectra are of interest. However, to avoid overloading this paper, only K spectra will be displayed due to their particular relevance. We are now going to systematically investigate how the approximation formalism presented in Secs. III and IV behaves in practice, using the test cases presented in Sec. II. Computer programs in which this formalism is implemented are available on request.

V. RESULTS

In this paper, OS and SES trajectories are obtained by using a standard fourth-order Runge-Kutta algorithm. OS trajectories are obtained by integrating the equations of the original system while SES trajectories are obtained by integrating the OS and applying the DST to each sampled point. SRS trajectories are obtained by using the form (92) with a variable step-size algorithm and routine taken from [31]. Except when explicitly stated otherwise, displayed trajectories last for $100T_0$ with a sampling rate of 100 points per T_0, in which T_0 is the pseudoperiod of the attractors (T_0 is about 6.2, 0.73, and 2.7 for the Rössler system, the Lorenz system, and the TLO model, respectively; it may be shown that OS and SS own the same pseudoperiod). Before recording trajectory data, transients are killed during $100T_0$.

Reconstruction spectra are evaluated by running the OS with a fourth-order Runge-Kutta routine, with constant time step δt. This same time step is used to evaluate standard coordinates according to a second-order centered finite difference scheme. The reconstruction also depends on N_q, the number of points on the net, N_s, the number of net points sampled per T_0, and N_p, the number of retained polynomials. The vector $(\delta t, N_q, N_s, N_p)$ is called the (reconstruction) driving vector. All displayed K spectra are presented under the form

$K_j^+ = \epsilon |K_j|^a$ in which ϵ is $\mathrm{sgn}(K_j)$ and a is conveniently chosen to better emphasize the features of the spectrum when spectrum components exhibit big differences in their order of magnitude.

A. Rössler system, observable x

The OS and the SES are displayed in Figs. 1 and 2, respectively. Although the SEF takes the form of a rational function, reconstructions are found to be very easy and robust, i.e., exhibiting a very small sensitivity with respect to the driving vector. Very satisfactory results are regularly obtained by using $N_p = 33 - 38$ and 47. Even with $N_p = 6$ polynomials, the general structure of the SES with a bit of fractality may be observed, although in this case the SRS does not compare favorably enough with the SES. Due to such a strong robustness, successful reconstructions may be obtained by decreasing N_q to small values. In Fig. 3, we provide an example with a driving vector equal to $(10^{-3}, 500, 5, 33)$, i.e., the original system has been sampled over $100T_0$. It is possible to obtain satisfactory reconstruction by sampling over a smaller number of pseudoperiods if both N_q and N_s are increased in an adequate way, i.e., by oversampling. It is certainly remarkable that the rational function of the SES may be correctly approximated by using only 33 polynomials (i.e., 33 components in the K spectrum) with such a limited amount of data. With driving vectors of the form $(10^{-3}, 100, 5, N_p)$ no satisfactory reconstructions are obtained, but SRS's still may exhibit periodic orbits or fractal orbits well reminiscent of the SES attractor. A K spectrum is displayed in Fig. 4 for $N_p = 100$. It is clear that the relevant information is contained in the range $j < 50$, in agreement with previous comments. There is also some information around $j = 60$ but it is likely to be parasitic because reconstructions with $N_p \approx 60$ are no more successful. Let us also note that taking more polynomials than necessary not only adds parasitic K_j's but also spoils the small order K_j's.
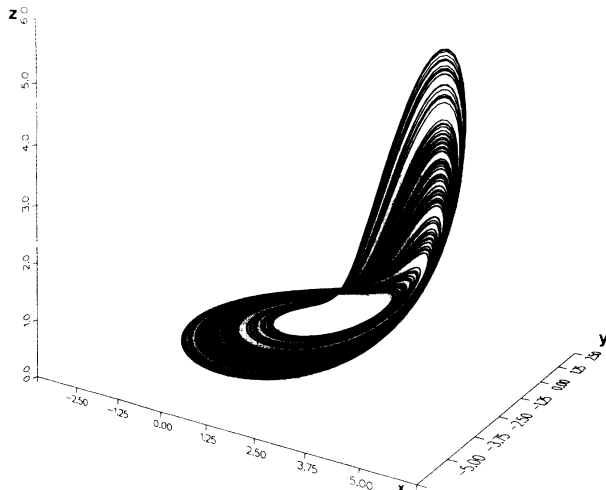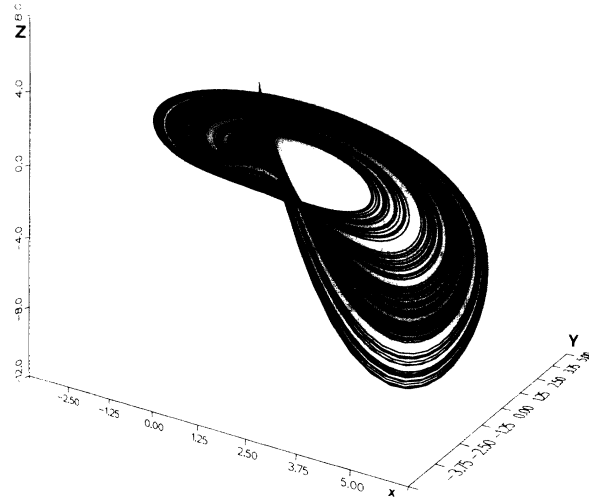
FIG. 2. Rössler system, observable x, SES.
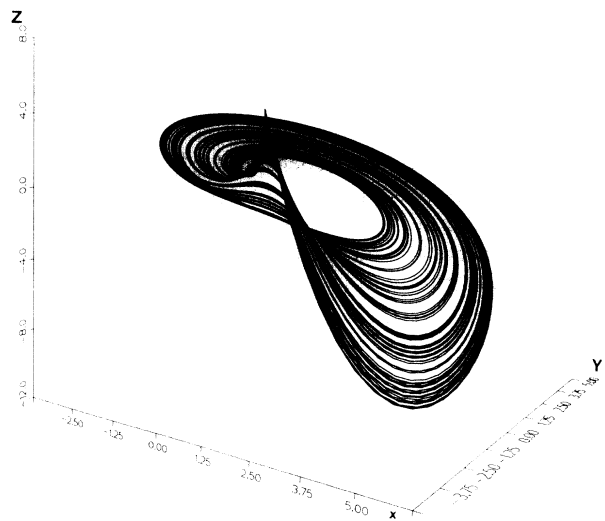
FIG. 3. Rössler system, observable x, SRS with driving vector $(10^{-3}, 500, 5, 33)$.

FIG. 1. Rössler system, observable x, OS.
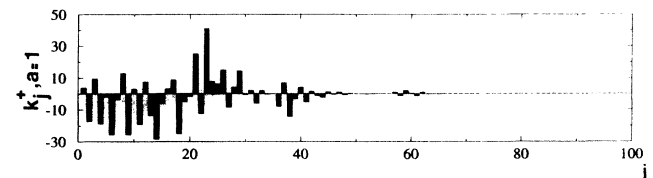
FIG. 4. Rössler system, observable x, K spectrum with driving vector $(10^{-3}, 10^5, 100, 100)$.
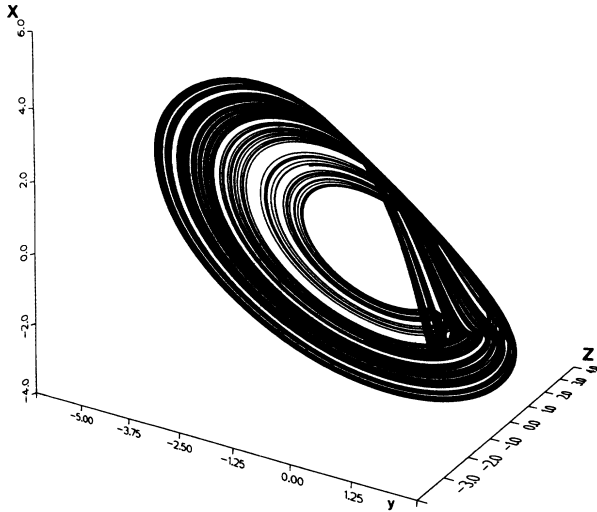
FIG. 5. Rössler system, observable y, SES.

B. Rössler system, observable y

The SES is displayed in Fig. 5. It is recalled that the SEF in this case is indeed a polynomial. Therefore the SRF in our algorithm exhibits the same mathematical structure as the SEF. As a consequence, reconstructions in this case are found to be exceptionally robust. It is also possible to readily compare the reconstructed K spectrum and the exact one. With standard coordinates reading (y,Z,X), the SEF given in Eq. (12) also reads

$$F^* = K_1 + K_2 y + K_3 Z + K_4 X + K_5 y^2 + K_6 yZ$$
$$+ K_7 yX + K_8 Z^2 + K_9 ZX , \qquad (94)$$

from which the exact K spectrum is obtained by identification, explicitly showing that only nine polynomials are required for the SRF. It has been possible to obtain perfect reconstructions by decreasing N_q down to such a small value as 10. An example is provided in Fig. 6 for a driving vector equal to $(10^{-3},10,10,10)$, i.e.,
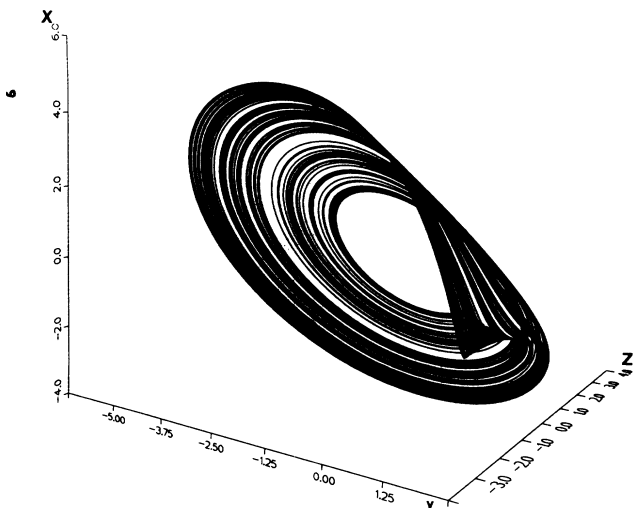
representing a sampling over only one pseudoperiod. It is also certainly remarkable that sampling over only one pseudoperiod is enough to reproduce the fractal structure of the system which can only be apparent by integrating it over a large number of pseudoperiods. We did not succeed in reconstructing the system with only $N_q = 9$. The smallest successful value $N_q = 10$ is just the number of required polynomials, i.e., 9, plus one, i.e., nearly identical to the theoretical limit discussed in Sec. IV E.

Calling K_i and K_i^* the components of the exact and reconstructed K spectra, respectively, we may define relative errors ϵ_i according to

$$\epsilon_i = \frac{|K_i - K_i^*|}{K_i} . \qquad (95)$$

In the case of Fig. 6, for $i \in 1, \ldots, 9$, the ϵ_i's range between 0.000 60% and 0.0039%, with an arithmetic average equal to 0.0015%. For K_{10}, which is theoretically equal to 0, we have $K_{10}^* \approx 10^{-6}$, a very small value, indeed. Such a high degree of accuracy does not make it useful to present K spectra.

C. Rössler system, observable z

The SES is displayed in Fig. 7. Many runs with various driving vectors have been carried out but no successful reconstructions have been obtained in this case, even by increasing N_q up to 10^7 (representing a rather extravagant amount of data, indeed). It however regularly happens that some SRS's that are reminiscent of the SES may be obtained in the same manner as in Fig. 8 (transients not killed) for a driving vector equal to $(10^{-2},10^6,1,63)$. Such SRS's generally correspond to N_p roughly equal to 60, say, in the range (55,70). The K spectrum in Fig. 9 indeed shows that some information is present for $j \approx 60$. It is likely that this information is not parasitic in this case, but essential to the quality of the reconstruction. Unfortunately, when the required number of polynomials increases too much, an accurate evaluation of the K spectra becomes more and more difficult

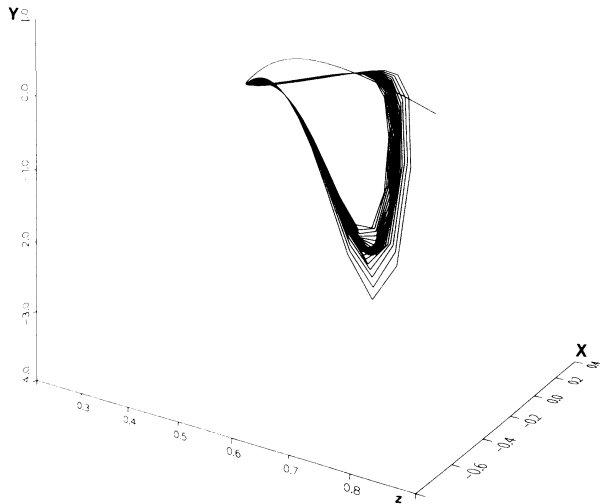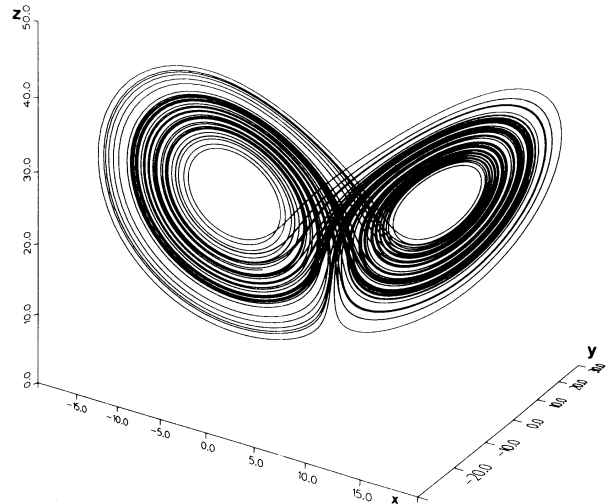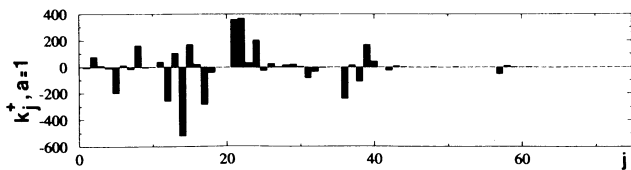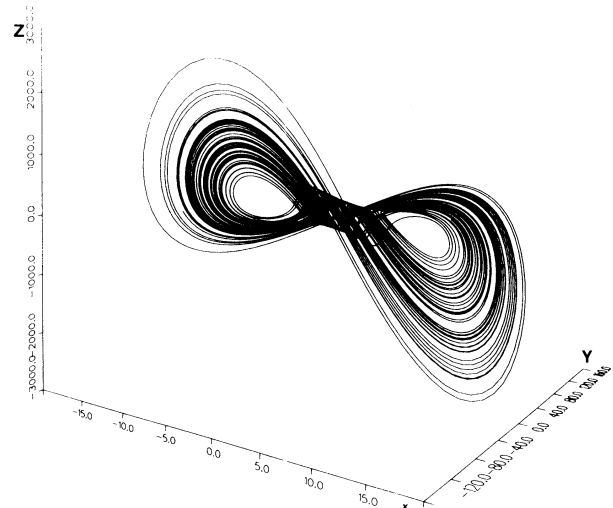FIG. 6. Rössler system, observable y, SRS with driving vector $(10^{-3},10,10,10)$.
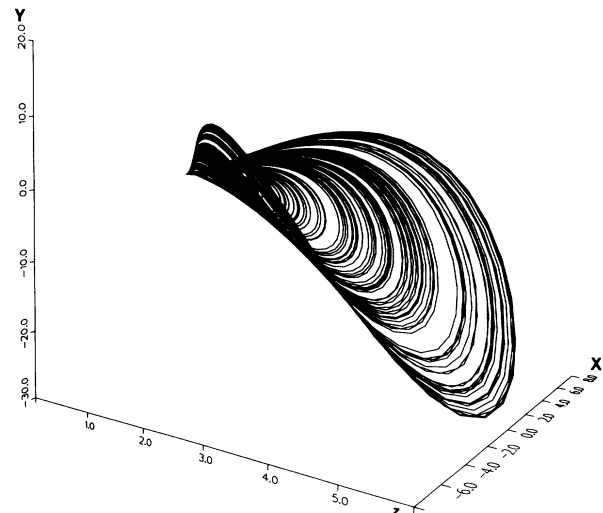
FIG. 7. Rössler system, observable z, SES.

FIG. 8. Rössler system, observable z, SRS with driving vector $(10^{-2}, 10^6, 1, 63)$.

FIG. 9. Rössler system, observable z, K spectrum with driving vector $(10^{-3}, 10^5, 100, 75)$.

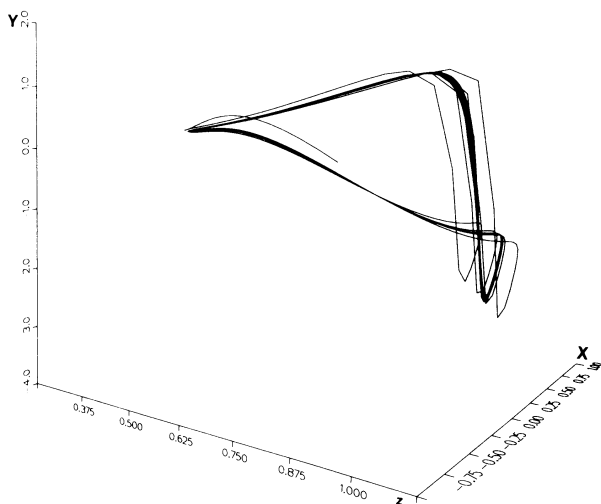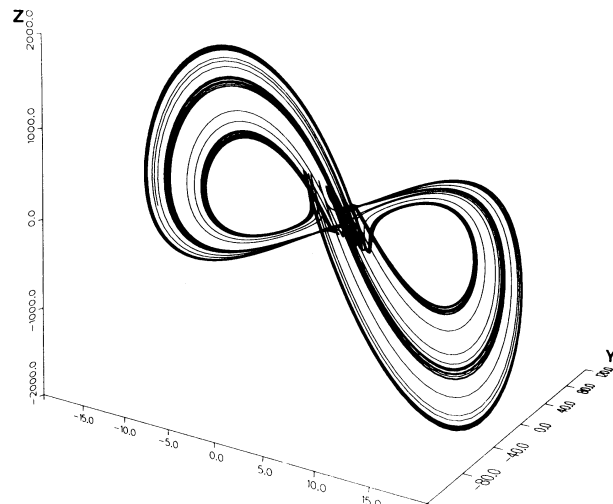FIG. 10. Rössler system, observable z, SRS with driving vector $(10^{-2}, 10^7, 1, 200)$.

FIG. 11. Lorenz system, observable x, OS.

FIG. 12. Lorenz system, observable x, SES.

FIG. 13. Lorenz system, observable x, SRS with driving vector $(10^{-2}, 10^4, 1, 18)$.

for two reasons: (i) the order of the moments involved in our algorithm increases (see Sec. IV F) and therefore their evaluation requires to increase the size of the net to provide accurate enough statistics, and (ii) the algorithm proceeding recursively, errors accumulate when higher-order polynomials are evaluated. Therefore, in some cases, the required value of N_q may be too great to be in practice affordable. This is illustrated by commenting on a last run with driving vector $(10^{-2}, 10^7, 1, N_p)$. With such a big value of $N_q = 10^7$, structures reminiscent of the SES are observed for nearly all N_p's in the range (60,200), with the example for $N_p = 200$ displayed in Fig. 10 (transients not killed). The lower limit of this N_p range, i.e., 60, confirms the relevance of the information in the K spectrum for $j \approx 60$, and the robustness of the structure of Fig. 10 when N_p is varied in the range indicates that higher-order polynomials do not add significant parasitic contributions to the K spectrum.

D. Lorenz system, observable x

The OS and SES are displayed in Figs. 11 and 12, respectively. Let us note the very big disparity in coordinate scales exhibited by the SES. From many runs, it is observed that reconstructions leading to structures reminiscent of the SES are regularly obtained for $N_p = 18$. An example is provided in Fig. 13 (transients not killed) for a driving vector equal to $(10^{-2}, 10^4, 1, 18)$. Such structures usually lead to small-order limit cycles without any fractal structure when transients are killed. They have essentially been observed only for a limited number of N_p's, namely, 14, 15, and 18, up to $N_q = 10^7$. Therefore, these N_p values play a special role. The value $N_p = 18$ seems to be the most interesting, because fairly good fractal reconstructions may be obtained in this case with an example in Fig. 14 for $(10^{-3}, 10^4, 100, 18)$. Unfortunately, such reconstructions are not robust with respect to a change in the driving vector. As an example, a run with a dense net $(N_q = 10^8)$ has finally been carried out
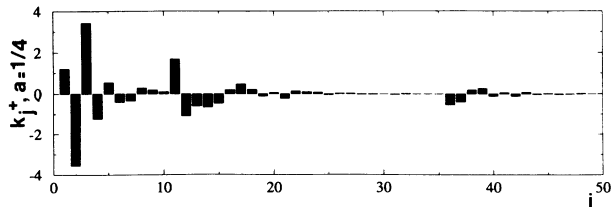

FIG. 15. Lorenz system, observable x, K spectrum with driving vector $(10^{-3}, 10^5, 100, 50)$.
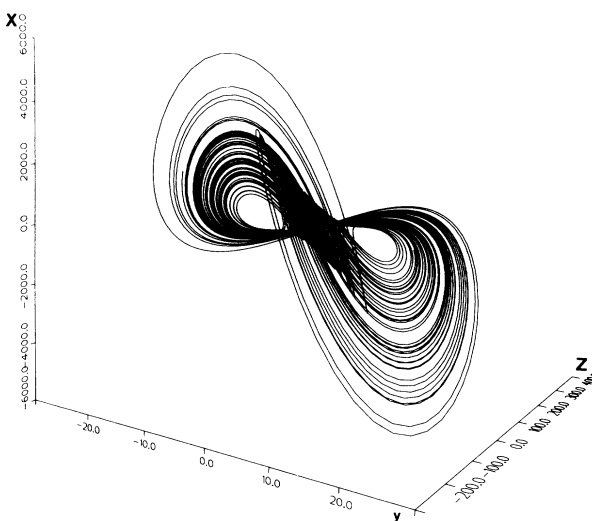

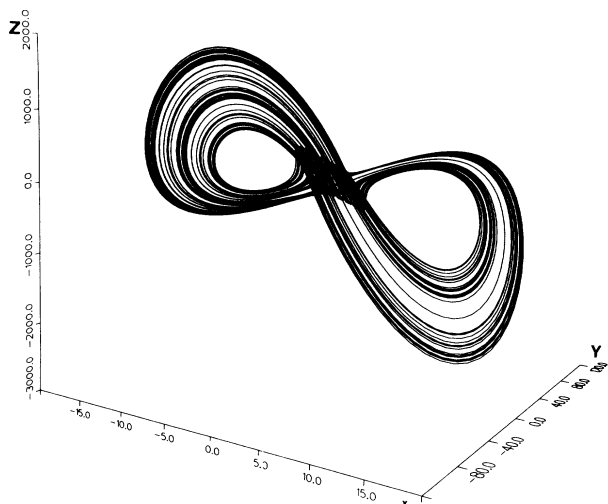FIG. 16. Lorenz system, observable y, SES.

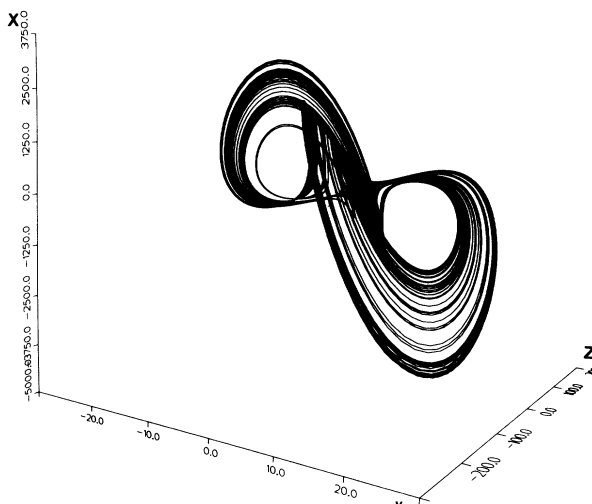FIG. 14. Lorenz system, observable x, SRS with driving vector $(10^{-3}, 10^4, 100, 18)$.

FIG. 17. Lorenz system, observable y, SRS with driving vector $(10^{-3}, 10^4, 100, 47)$.

with driving vector $(10^{-4}, 10^8, 100, N_p)$ for N_p up to 100. For such a big N_q, structures reminiscent of the SES are obtained for nearly all N_p's but without any fractal structures. A K spectrum is given in Fig. 15 showing that most of the information is contained in a small number of polynomials. The peak for $j = 18$ is small but the corresponding polynomial is expected to be essential. It is likely that the difficulty in obtaining robust fractal reconstructions for this case is partly associated with the big disparity in scale coordinates.

E. Lorenz system, observable y

The SES is displayed in Fig. 16, exhibiting a strong similitude with the SES from variable x, including a big disparity in coordinate scales. Reconstructions are robust in the weak sense, i.e., structures reminiscent of the SES are regularly obtained for nearly all N_p's, in contrast with the case of variable x for which $N_p = 14$, 15, and 18 were privileged. Also, rather satisfactory fractal reconstructions are regularly obtained with an example in Fig. 17 for a driving vector equal to $(10^{-3}, 10^4, 100, 47)$. We even succeeded in obtaining a fairly good reconstruction with only $N_p = 13$ polynomials for $(10^{-2}, 10^5, 1, 13)$. Unfortunately, such fractal reconstructions are not robust. It is again likely that N_q values should be increased to extravagant values to provide a satisfactory convergence. In particular, clues to convergence are observed for $N_q = 10^7$, with a driving vector $(10^{-3}, 10^7, 1, N_p)$. In this case, a rather satisfactory reconstruction is observed for $N_p = 44$ (Fig. 18) and other fractal reconstructions, although much less satisfactory, are observed for N_p from 56 up to 82. A K spectrum is shown in Fig. 19, presenting many similarities with the K spectrum for observable x. It is again likely that the difficulty in obtaining robust fractal reconstructions for this case is partly associated with the big disparity in scale coordinates.

F. Lorenz system, observable z

The SES is displayed in Fig. 20. In contrast with the OS, and SES's with variables x and y, this attractor displays only one wing. This is an interesting point because, considering the symmetry of the Lorenz vector field $(x \rightarrow -x, y \rightarrow -y)$, Rössler [32] stated that "a trick which exploits the inherent . . . symmetry between the two leaves of the flow, so that in effect only a single leaf needs to be considered has yet to be found." He then went on by publishing his so-called Rössler system leading to a chaotic motion on a single band. Because the Lorenz system is a model, he stated that his system is a "model of a model," therefore emphasizing the fact that he was indeed looking for a reduction from the two-leaf motion in the Lorenz system to a single-leaf motion. It therefore appears that SS's (SES and SRS's) naturally provide the trick asked for by Rössler.

Let us note that there is still a big disparity in coordinate scales. However, in this case, probably in connection with the simple structure of the flow (although the SES vector field was so complicated that we decided not to write it down), reconstructions are very robust. Very satisfactory reconstructions are obtained with nearly no
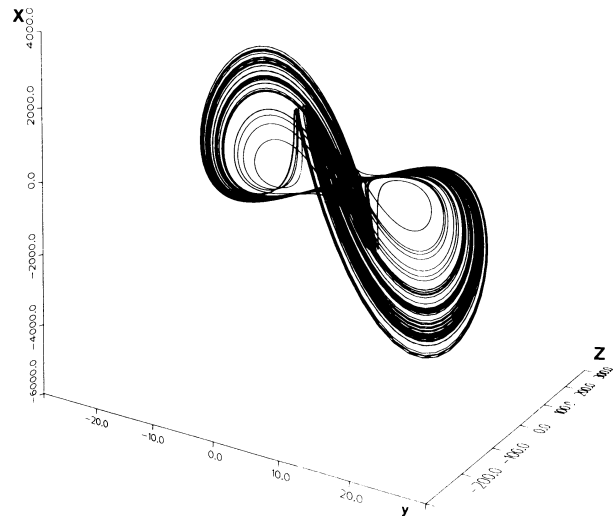

FIG. 18. Lorenz system, observable y, SRS with driving vector $(10^{-3}, 10^7, 1, 44)$.
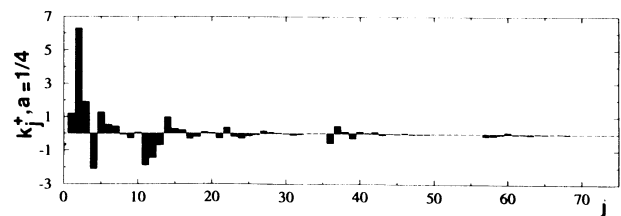

FIG. 19. Lorenz system, observable y, K spectrum with driving vector $(10^{-3}, 10^5, 100, 75)$.
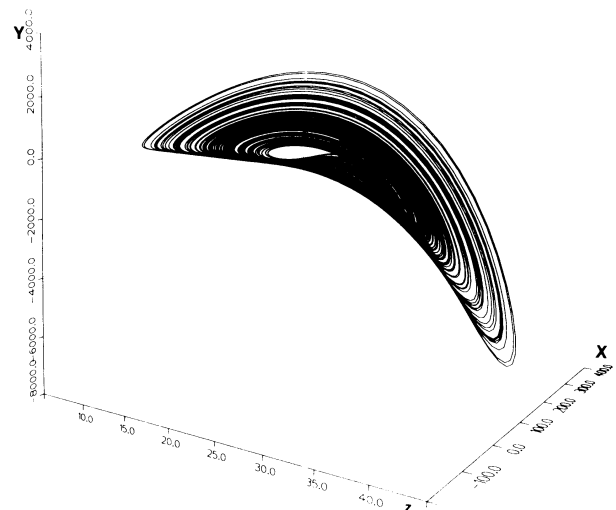

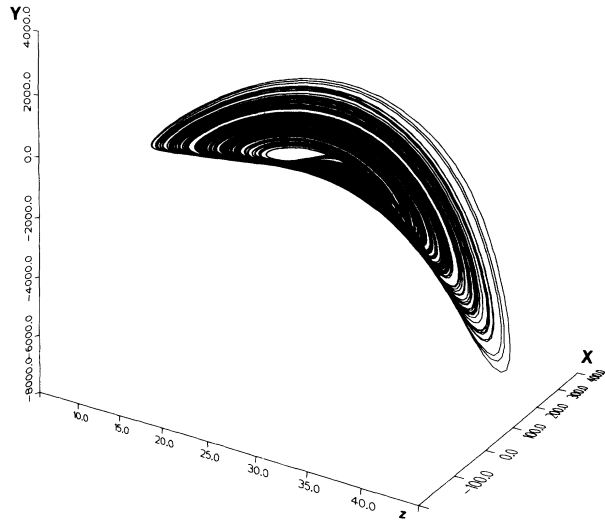FIG. 20. Lorenz system, observable z, SES.

FIG. 21. Lorenz system, observable z, SRS with driving vector $(10^{-3}, 10^4, 100, 46)$.
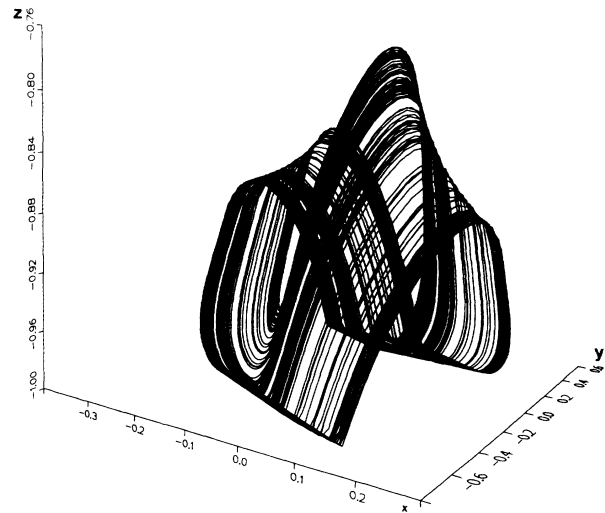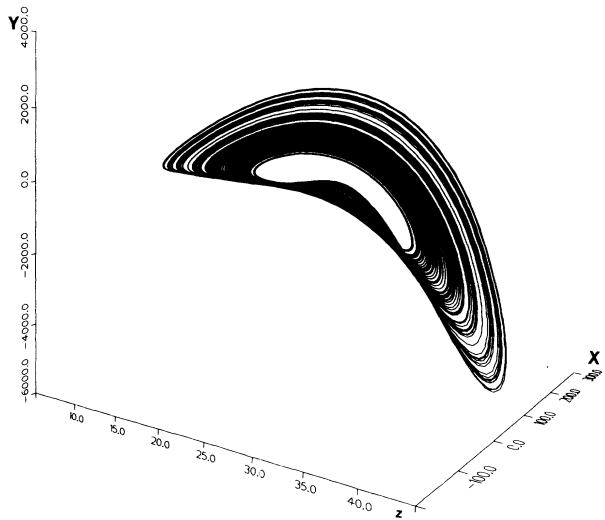
FIG. 24. TLO system, observable x, OS.

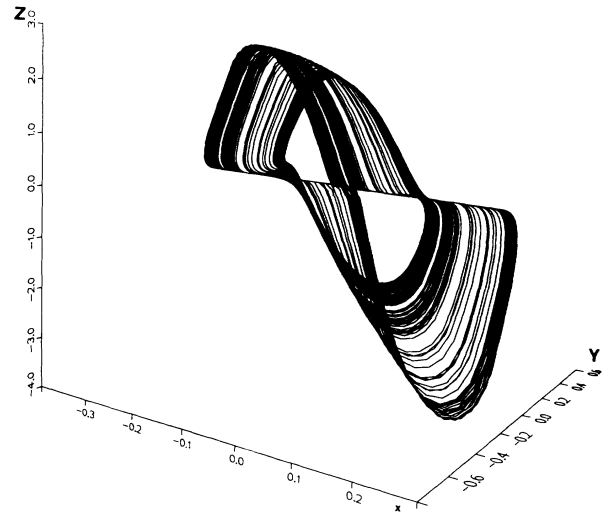FIG. 22. Lorenz system, observable z, SRS with driving vector $(5.10^{-4}, 10^2, 1, 50)$.

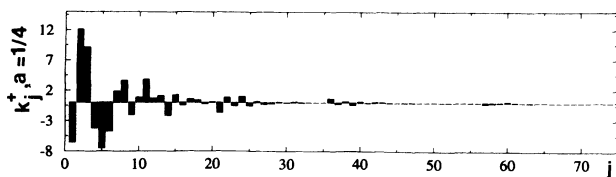FIG. 25. TLO system, observable x, SES.

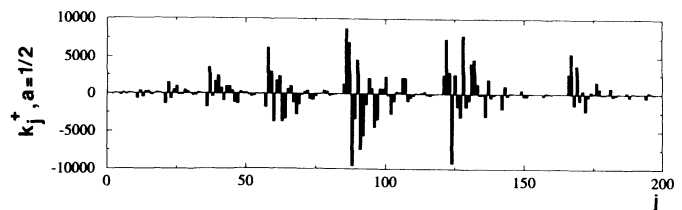FIG. 23. Lorenz system, observable z, K spectrum with driving vector $(10^{-3}, 10^5, 100, 75)$.

FIG. 26. TLO system, observable x, K spectrum with driving vector $(10^{-3}, 10^4, 10^3, 200)$.

dependence on the driving vector, for $N_p \in \approx (46,59)$. An example is provided in Fig. 21 for a driving vector equal to $(10^{-3},10^4,100,46)$. Due to the strong robustness for this case, it is possible to decrease N_q to very small values, with an example in Fig. 22 for $(5.10^{-4},100,1,50)$, although some deterioration with respect to the previous figure may be observed. The K spectrum exemplified in Fig. 23 is well correlated with the above remarks. Although most components are obtained for $j < 35$, the small components for $j > 35$ must be essential to the quality of the reconstructions.

G. TLO model

For the vector field of Eq. (22), the OS and the SES are displayed in Figs. 24 and 25, respectively. The flat bands in these attractors are associated with the sharp cutoff term in the vector field and expectedly make this case a very acid test. Expected difficulties are well confirmed by the complex structure of the K spectrum (Fig. 26), exhibiting many disjoined bursts of peaks spreading up to (at least) $j = 200$. Indeed, we did not succeed in satisfactorily solving this case even after having systematically tested several thousands of driving vectors.

Most of the time, a limit cycle, however not well reminiscent of the SES, is obtained by using only $N_p = 11$ polynomials. Many limit cycles, now well reminiscent of the SES skeleton, are regularly observed for $N_p \in [23,48]$, possibly period doubled, as illustrated in Fig. 27 for $(10^{-3},10^6,2000,23)$ representing a sampling over $500 T_0$ and Fig. 28 for $(10^{-3},10^6,2,24)$ representing a sampling over $500\,000 T_0$. The value $N_p = 47$ deserves a special mention because it regularly provides structures very well reminiscent of the SES, looking like transient chaos, but eventually converging to simple limit cycles of order 1 or 2, or diverging. An example is shown in Fig. 29 for $(10^{-3},10^7,100,47)$ in which transients have been killed for $20 T_0$. This trajectory, however, diverges after about $150 T_0$. The best no-diverging trajectory which is, however, very far from being fully satisfactory (Fig. 30) has
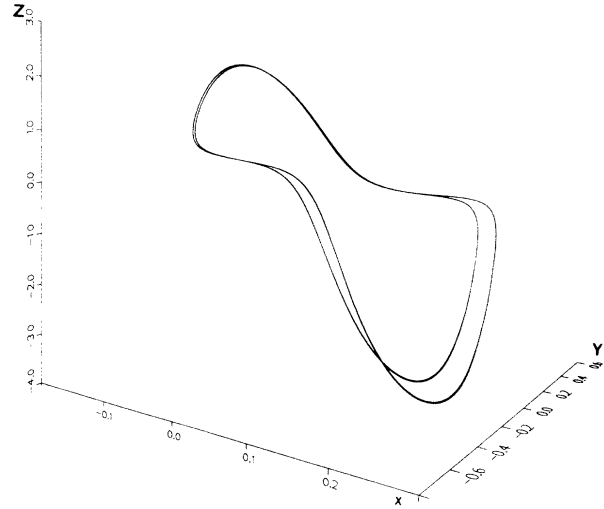

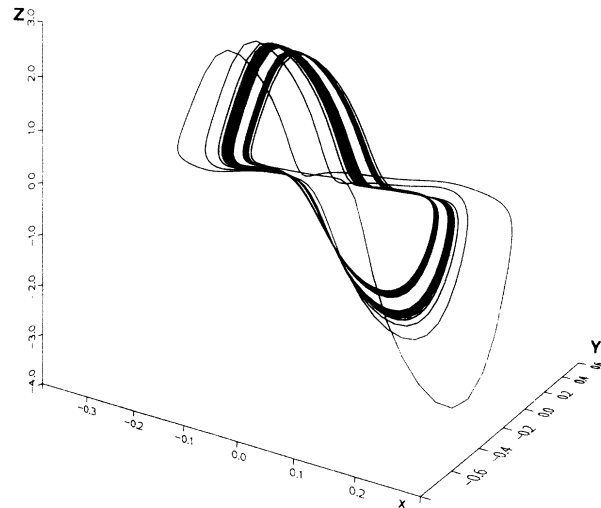FIG. 28. TLO system, observable x, SRS with driving vector $(10^{-3},10^6,2,24)$.

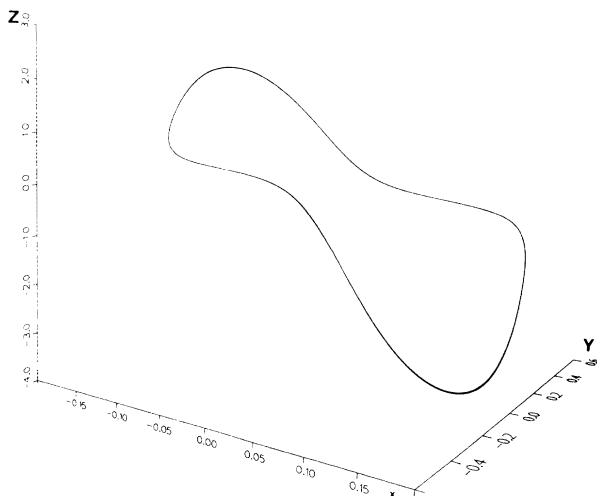FIG. 29. TLO system, observable x, SRS with driving vector $(10^{-3},10^7,100,47)$.

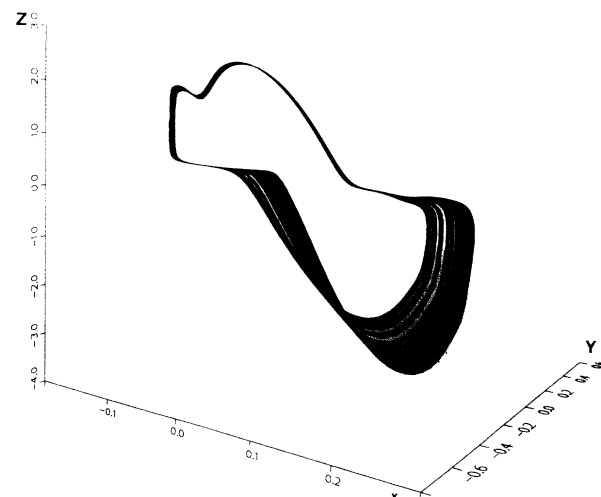FIG. 27. TLO system, observable x, SRS with driving vector $(10^{-3},10^6,2000,23)$.

FIG. 30. TLO system, observable x, SRS with driving vector $(10^{-3},10^6,10^3,165)$.

been obtained with a big number of polynomials, for $(10^{-3}, 10^6, 10^3, 165)$. Such a big value of N_p is associated with the rightmost burst of peaks in the K spectrum. It is therefore likely that such a difficult case would require a large number of polynomials, which in turn, as previously discussed, would require extravagant values of N_q. In particular, runs with $N_q = 10^7$ and 10^8 have been carried out without leading to noticeable improvements.

VI. CONCLUSION

We have presented a global vector-field reconstruction technique relying on standard systems in which the so-called standard function is approximated by using a multivariate L_2-polynomial approximation on nets. Several test cases have been investigated. These test cases may be separated into three classes: (i) a class for which reconstructions are easy and robust, allowing very satisfactory results with a very small amount of data, including the Rössler system, with observables x and y, and the Lorenz system with variable z; (ii) a class for which rather satisfactory reconstructions are obtained but in a no-robust way, including the Lorenz system, with observables x and y; and (iii) a class for which no satisfactory reconstructions are obtained, although some structures reminiscent of the correct one may be produced, including the Rössler system with observable z and the TLO system with variable x. Validations relied on the comparison between SES and SRS graphical displays but could have also relied on the comparison between invariants such as generalized dimensions as done in our previous works [9–13].

Some indications on future works are now provided. Although our technique relies on standard systems, the approximation technique itself could be used in other approaches, such as using eigenfunctions generated by SVD or for map reconstructions and forecasting. For a given system, reconstructions are more or less easy, depending on the chosen observable. This fact suggests that, for a given observable x, easier reconstruction might be possible by using a derived observable $f(x)$ with the proviso

to know how to choose a best function f. More generally, generalized standard systems might be introduced in which the first components of the SS vector field would be given by known functions of the standard coordinates with again a single standard function to be determined. In particular, when the standard coordinate scales are very different, such as for the Lorenz system, such generalized standard systems may be easily derived in order to renormalize the scales. This leads to so-called squeezed systems that we previously used to decrease biases involved in generalized dimension computations [9–13].

Also, the approximation technique presented in this paper can likely be improved, for instance, by using a perturbation procedure in which, a first approximation of the standard function being obtained, a second step using again our polynomial procedure could be used to improve the approximation. The first approximation could be chosen by selecting the most significant polynomials. Systems pertaining to classes (ii) and (iii) should be selected as test cases for checking improved methods. In particular, the TLO system provides a particularly interesting acid test.

When using rational functions, the method was not very robust with respect to the presence of noise (although it could, however, afford a bit of it), due to the presence of aforementioned singularities. The present technique without any singularity should perform much better. Of course, a prior step should concern noise removal, for instance, by using Fourier filtering, wavelet transform filtering, or SVD filtering, among others.

All these lines of research are now to be investigated and should eventually provide a new tool of interest for the study of experimental data, including the automatic production of phenomenological models and forecasting techniques for flows (and maps).

ACKNOWLEDGMENTS

[1] N. H. Packard, J. P. Crutchfield, J. D. Farmer, and R. S. Shaw, Phys. Rev. Lett. **45**, 712 (1980).
[2] J. P. Crutchfield and B. S. McNamara, Complex Syst. **1**, 417 (1987).
[3] J. D. Farmer and J. J. Sidorowich, Phys. Rev. Lett. **59**, 845 (1987).
[4] H. Whitney, J. Math. **37**, 645 (1936).
[5] H. Whitney, Ann. Math. **45**, 220 (1944).
[6] R. Mañé, in *Dynamical Systems and Turbulence* (Warwick, 1980), edited by D. A. Rand and L. S. Young, Lecture Notes in Mathematics Vol. 898 (Springer-Verlag, Berlin, 1981), pp. 230–242.
[7] F. Takens, in *Dynamical Systems and Turbulence*, Ref. [6], p. 366.
[8] F. Takens, in *Nonlinear Dynamics and Turbulence*, edited by G. I. Barenblatt, G. Iooss, and D. D. Joseph (Pitman, New York, 1983), p. 314.
[9] G. Gouesbet, Phys. Rev. A **43**, 5321 (1991).
[10] G. Gouesbet, Phys. Rev. A **44**, 6264 (1991).
[11] G. Gouesbet (unpublished).
[12] G. Gouesbet, Phys. Rev. A **46**, 1784 (1992).
[13] G. Gouesbet and J. Maquet, Physica D **58**, 202 (1992).
[14] G. Rowlands and J. C. Sprott, Physica D **58**, 251 (1992).
[15] A. K. Agarwal, D. P. Ahalpara, P. K. Kaw, H. R. Prablakera, and A. Sen, J. Phys. **35**, 287 (1990).
[16] M. Palus and I. Dvorák, Physica D **55**, 221 (1992).
[17] G. B. Mindlin, H. G. Solari, M. A. Natiello, R. Gilmore, and X. J. Hou, J. Nonlinear Sci. **1**, 147 (1991).
[18] M. Casdagli, S. Eubank, J. D. Farmer, and J. Gibson, Physica D **51**, 52 (1991).

[19] J. F. Gibson, J. D. Farmer, M. Casdagli, and S. Eubank, Physica D **57**, 1 (1992).

[20] J. R. Rice, *The Approximation of Functions* (Addison-Wesley, Reading, MA, 1964), Vol. 1; (1969), Vol. 2.

[21] J. Cremers and A. Hübler, Z. Naturforsch. A **42**, 797 (1987).

[22] J. L. Breeden and A. Hübler, Phys. Rev. A **42**, 5817 (1990).

[23] J. Guckenheimer and P. Holmes, *Nonlinear Oscillations, Dynamical Systems, and Bifurcations of Vector Fields*, Applied Mathematical Sciences Vol. 42 (Springer, Berlin, 1983).

[24] J. M. T. Thompson and H. B. Stewart, *Nonlinear Dynamics and Chaos* (Wiley, New York, 1987).

[25] E. N. Lorenz, J. Atmos. Sci. **20**, 130 (1963).

[26] S. Meunier-Guttin-Cluzel, B. Maheu, and G. Gouesbet, Physica D **58**, 423 (1992).

[27] E. Ringuet, C. Rozé, G. Gouesbet, Phys. Rev. E **47**, 1405 (1993).

[28] G. Gouesbet, Phys. Rev. A **42**, 5928 (1990).

[29] G. Dahlquist and A. Björck, *Numerical Methods* (Prentice-Hall, Englewood Cliffs, NJ, 1974), Chap. 4.

[30] M. Giona, F. Lentini, and V. Cimagalli, Phys. Rev. A **44**, 3496 (1991).

[31] W. H. Press, B. P. Flannery, S. A. Teukolsky, and W. T. Vetterling, *Numerical Recipes, The Art of Scientific Computing* (Cambridge University Press, Cambridge, England, 1986), Sec. 15.2, pp. 554–560.

[32] O. E. Rössler, Phys. Lett. A **57**, 397 (1976).